Decoherence-Resilient Linear Optical Two-Qubit Quantum Gate

Michal Mičuda, Robert Stárek, Jaromír Fiurášek,* and Radim Filip
Department of Optics, Palacký University, 17. listopadu 1192/12, 771 46 Olomouc, Czech Republic

(Received 16 April 2020; revised 26 July 2020; accepted 6 November 2020; published 25 November 2020)

Quantum information can be protected from noise and decoherence by encoding it into a decoherence-free subspace of the full Hilbert space. In this approach, it is important to devise implementations of quantum logic gates acting on the encoded logical qubits. Here, we experimentally investigate the implementation of an entangling linear optical controlled-Z gate on two logical qubits encoded into pairs of physical qubits, which protects the quantum information from collective dephasing. This decoherence-resilient two-qubit gate on logical qubits is realized using a suitable four-qubit quantum gate on the physical qubits, which may help to protect the encoded quantum information from systematic errors arising due to imperfect operations on single logical qubits. We characterize the gate operation on input superposition states and demonstrate its ability to protect quantum coherence even under complete collective dephasing.

DOI: 10.1103/PhysRevApplied.14.054066

I. INTRODUCTION

The operation of large-scale quantum-information processors is extremely challenging due to noise and decoherence, which destroy the quantum coherence of complex entangled states. While, in the early days of quantum-information science, it seemed that these obstacles were insurmountable, it later turned out that a certain amount of noise and decoherence can be tolerated. Using quantum error correction [1–6] and encoding each logical qubit into several physical qubits, one can, in principle, construct a scalable quantum computer [7] that can faithfully operate even in the presence of a nonvanishing amount of noise. Although the tolerable noise levels are typically very low or the required overheads dauntingly high (although scaling polynomially) [8], this insight still provides an extremely strong motivation for the theoretical and experimental development of quantum-information processing devices with ever-increasing complexity [9,10].

The required overheads and complexity of logical qubit encoding can be significantly reduced if it is only necessary to protect the qubits from some specific dominant noise or decoherence and not from arbitrary generic errors [11–19]. A simple yet fundamentally important example is provided by collective dephasing, which reduces the coherence between the computational basis states $|0\rangle$ and $|1\rangle$. If two physical qubits suffer from identical correlated random phase shifts, then one can identify a two-dimensional decoherence-free subspace [14,15,20–23] of the two-qubit space, which is not affected by the collective dephasing. A logical qubit protected from the collective dephasing can be encoded into this subspace spanned by the product states $|0_L\rangle = |0\rangle|1\rangle$ and $|1_L\rangle = |1\rangle|0\rangle$.

This encoding is very promising and suitable for optical quantum communication applications and has been explored in a host of experiments to enable faithful transfer of quantum states of photons and their protection under collective dephasing [21–24]. The next important step is experimental realization of decoherence-free quantum gates on the photonic logical qubits, as already experimentally demonstrated for stationary trapped-ion qubits [20]. Although an entangling controlled-Z (CZ) gate on two logical qubits can be implemented with a gate acting on two physical qubits only [20,25], it is also of interest to study alternative gate implementations, such as those utilizing inherently four-qubit gates. These approaches become inequivalent in the presence of implementation errors beyond collective dephasing and may lead, e.g., to different leakages from the decoherence-free subspace.

In this work, we experimentally demonstrate and investigate a linear-optical entangling quantum gate that is resilient to collective dephasing. Specifically, we utilize a modified version of a four-qubit controlled-controlled-controlled-Z (CCCZ) gate to implement an entangling gate on two logical qubits, each of which is encoded into a pair of physical qubits represented by the polarization and path degrees of freedom of a single photon. Our linear optical scheme provides a suitable test bed for the study of transformations of logical qubits with inherently multiqubit quantum gates, as it enables high versatility, purity, and precision of the quantum state preparations, transformations, and measurements. We experimentally confirm faithful implementation of the two-qubit entangling operation, insensitive to collective decoherence, and

*fiurasek@optics.upol.cz

we theoretically illustrate the different performances of schemes with entangling gates acting on two or four physical qubits in the presence of errors and imperfections beyond collective dephasing.

II. ENTANGLING GATE RESILIENT TO COLLECTIVE DEPHASING

The dephasing operation $\mathcal{D}_q$ acting on a single-qubit density matrix ρ is a unital completely positive map [4],

$$\mathcal{D}_q(\rho) = q\rho + (1-q)\sigma_Z\rho\sigma_Z, \tag{1}$$

where $\sigma_Z = |0\rangle\langle 0| - |1\rangle\langle 1|$ is the Pauli matrix describing unitary phase flip. The dephasing $\mathcal{D}_q$ succinctly describes the effect of random phase fluctuations. Any transformation

$$\rho \to \int_{-\pi}^{\pi} V(\phi)\rho V^{\dagger}(\phi)P(\phi)d\phi, \tag{2}$$

where $P(\phi)$ is a symmetric probability density, $P(-\phi) = P(\phi)$, and $V(\phi) = |0\rangle\langle 0| + e^{i\phi}|1\rangle\langle 1|$ can be represented by the map $\mathcal{D}_q$ with $q = \frac{1}{2} + \int_0^{\pi} P(\phi)\cos(\phi)d\phi$. The dephasing operation leaves the diagonal density-matrix elements in the computational basis unchanged, while the off-diagonal elements are attenuated by factor $2q-1$. The dephasing can be caused, e.g., by fluctuating classical fields or by interaction with the environment, which introduces correlations between the computational basis states of the system qubit and the environment:

$$|0\rangle|E_{\rm in}\rangle \to |0\rangle|E_0\rangle, \quad |1\rangle|E_{\rm in}\rangle \to |1\rangle|E_1\rangle. \tag{3}$$

In this latter case, $q = \frac{1}{2}(1 + |\langle E_0|E_1\rangle|)$.

Let us now consider the situation in which the dephasing is caused by fluctuating classical fields and the fluctuations are such that two physical qubits located sufficiently close to each other suffer from the same random phase shifts. Mathematically, the operation acting on the two-qubit state is a mixture of unitaries $V(\phi)\otimes V(\phi)$. A two-dimensional decoherence-free subspace spanned by the product states $|0_L\rangle = |0\rangle|1\rangle$ and $|1_L\rangle = |1\rangle|0\rangle$ is unaffected by such collective dephasing. Indeed, we have

$$\begin{aligned} &V(\phi)\otimes V(\phi)(\alpha|0\rangle|1\rangle + \beta|1\rangle|0\rangle) \\ &\quad = e^{i\phi}(\alpha|0\rangle|1\rangle + \beta|1\rangle|0\rangle); \end{aligned} \tag{4}$$

hence the logical qubit state $\alpha|0_L\rangle + \beta|1_L\rangle$ is protected and the overall phase shift $e^{i\phi}$ becomes physically irrelevant.

We note that this encoding is also applicable when the dephasing is caused by interaction with the environment [26], provided that the environment does not distinguish between the states $|01\rangle$ and $|10\rangle$ of two physical qubits and these two states couple to the environment in the same way. Assuming the collective interaction of two qubits with the environment in the form $|ij\rangle|E\rangle \to |ij\rangle|E_{ij}\rangle$, we require $|\langle E_{01}|E_{10}\rangle| = 1$.

In what follows, we investigate implementation of the two-qubit maximally entangling CZ gate on two logical qubits encoded in four physical qubits. We label the physical qubits with capital letters, with the first logical qubit encoded in physical qubits A and C and the second logical qubit encoded in physical qubits B and D. The CZ gate can be implemented by applying a two-qubit gate $U_{\rm CZ} = \exp(i\pi|11\rangle\langle 11|)$ to the first physical qubit of each logical qubit [20] [see Fig. 1(a)]. Here, we consider an alternative approach based on a quantum gate acting on all four physical qubits:

$$W = e^{i\pi|1_L1_L\rangle\langle 1_L1_L|} = e^{i\pi|1010\rangle\langle 1010|}. \tag{5}$$

Up to single-qubit bit flips, this transformation is equivalent to the four-qubit quantum CCCZ gate $U_{\rm CCCZ} = \exp(i\pi|1111\rangle\langle 1111|)$.

Under ideal conditions, gates $U_{\rm CZ}$ and W result in identical transformation of states of logical qubits. However, differences occur in the presence of errors and imperfections. Since these two gates act differently on states lying outside the decoherence-free subspace, they will introduce different systematic errors. To illustrate this, we consider the implementation of a CNOT gate on the two logical qubits by a sequence of gate $G_L = e^{i\pi H_G}$ acting on the second logical qubit, followed by gate $U_{\rm CZ}$ or W gate acting on both logical qubits, and finally an inverse gate $G_L^{\dagger}$ applied to the second logical qubit [see Fig. 1(b)]. Here,

$$H_G = \frac{1}{8}\left(\sigma_X\otimes\sigma_Y - \sigma_Y\otimes\sigma_X\right), \tag{6}$$

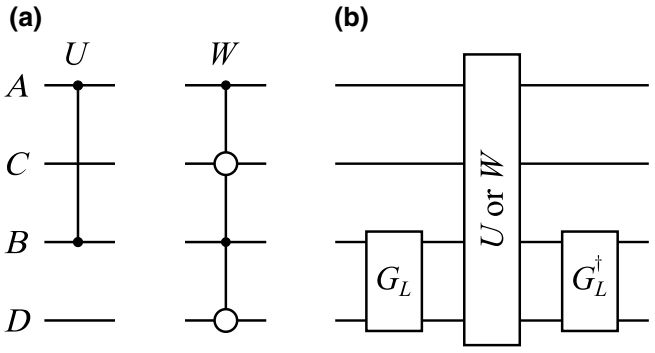

FIG. 1. (a) The implementation of entangling quantum gates on logical qubits encoded into pairs of physical qubits A, C and B, D. The CZ gate on logical qubits can be implemented either by applying a two-qubit gate $U_{\rm CZ}$ to physical qubits A and B or by applying a four-qubit gate W to all four physical qubits. (b) The implementation of a CNOT gate on logical qubits by a sequence of gate G_L on the second logical qubit, the CZ gate on the two logical qubits, and an inverse gate $G_L^{\dagger}$ on the second logical qubit.

expressed in terms of Pauli operators acting on the physical qubits, is a Hamiltonian that generates the required rotation of the second logical qubit, $G_L|0_L\rangle = |+_L\rangle$, $G_L|1_L\rangle = -|-_L\rangle$, where $|\pm_L\rangle = \frac{1}{\sqrt{2}}(|0_L\rangle \pm |1_L\rangle)$. To illustrate the differences in realistic performance for nonideal gates, we now consider a small distortion in the implementation of Hamiltonian H_G:

$$H_{G,\pm} = H_G + \frac{\kappa}{8}(\sigma_X \otimes I \pm I \otimes \sigma_X). \tag{7}$$

Let $G_{L,\pm} = e^{i\pi H_{G,\pm}}$. The resulting operations

$$\begin{aligned} C_U &= G^{\dagger}_{L,\pm,\mathrm{BD}} U_{\mathrm{CZ,AB}} G_{L,\pm,\mathrm{BD}}, \\ C_W &= G^{\dagger}_{L,\pm,\mathrm{BD}} W_{\mathrm{ABCD}} G_{L,\pm,\mathrm{BD}} \end{aligned} \tag{8}$$

do not fully preserve the states inside the decoherence-free subspace and their action on logical qubits deviates from that of the target CNOT gate U_{CNOT}. To quantify this, we define a projector onto the four-dimensional decoherence-free subspace of the two logical qubits:

$$\Pi_{\mathrm{DFS}} = \sum_{j=0}^{1}\sum_{k=0}^{1} |j_L\rangle\langle j_L|_{\mathrm{AC}} \otimes |k_L\rangle\langle k_L|_{\mathrm{BD}}. \tag{9}$$

A leakage from the decoherence-free subspace caused by gate S is quantified as

$$L = 1 - \frac{1}{4}\mathrm{Tr}\left[\Pi_{\mathrm{DFS}} S \Pi_{\mathrm{DFS}} S^{\dagger}\right]. \tag{10}$$

By definition, $L \geq 0$ and $L = 0$ if and only if the gate fully preserves the decoherence-free subspace, $S\Pi_{\mathrm{DFS}}S^{\dagger} = \Pi_{\mathrm{DFS}}$. We also introduce the difference between the actual operation on the decoherence-free subspace induced by some gate S and the ideal CNOT gate $U_{\mathrm{CNOT},L}$ on the logical qubits:

$$D = 1 - \frac{1}{16}\left|\mathrm{Tr}\left[\Pi_{\mathrm{DFS}} S \Pi_{\mathrm{DFS}} U^{\dagger}_{\mathrm{CNOT},L}\right]\right|^2. \tag{11}$$

Clearly, $D \geq 0$ and $D = 0$ only if $\Pi_{\mathrm{DFS}} S \Pi_{\mathrm{DFS}} = U_{\mathrm{CNOT},L}$. With the use of L and D, we can calculate the fidelity of the operation implemented on the decoherence-free subspace [27–29], which we define as a normalized overlap of the actually realized operation projected onto the decoherence-free subspace, $\tilde{S} = \Pi_{\mathrm{DFS}} S \Pi_{\mathrm{DFS}}$, and that of the ideal CNOT gate on the decoherence-free subspace,

$$F = \frac{\left|\mathrm{Tr}(\tilde{S}U^{\dagger}_{\mathrm{CNOT},L})\right|^2}{4\mathrm{Tr}(\tilde{S}\tilde{S}^{\dagger})} = \frac{1-D}{1-L}. \tag{12}$$

In Fig. 2, we plot the dependence of L, D, and F on κ for the gates C_U and C_W. We can see that the average imperfections induced by distortion in the implementation of the

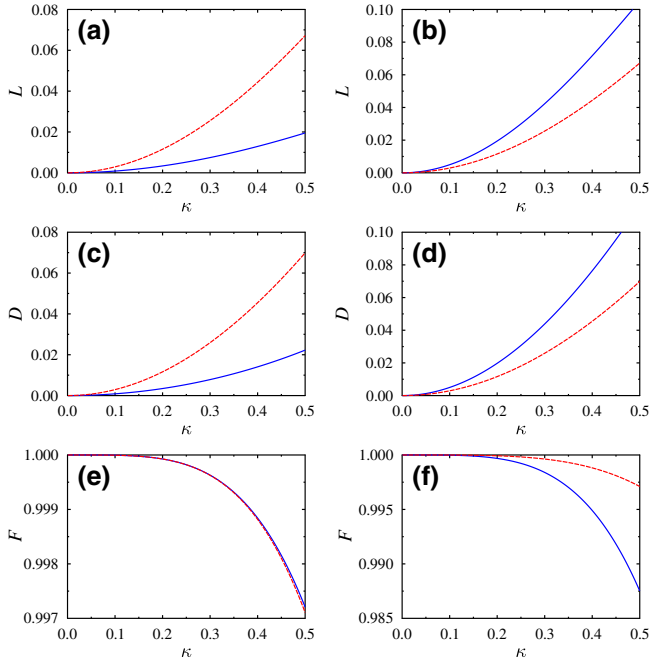

FIG. 2. The leakage L from the decoherence-free subspace (a),(b), the difference D between the actually implemented operation and the ideal CNOT gate on the logical qubits (c),(d), and the fidelity F of the quantum operation implemented on the decoherence-free subspace (e),(f) are plotted as functions of κ, which quantifies the strength of distortion of Hamiltonian H_G. The results are shown for the gates C_W (blue solid line) and C_U (red dashed line) and for two kinds of Hamiltonian distortions, $H_{G,+}$ (a),(c),(e) and $H_{G,-}$ (b),(d),(f).

Hamiltonian H_G differ for U_{CZ} and W and that the optimal choice depends on the particular form of the distortion. For $H_{G,+}$, the choice of the central gate W in the logic circuit in Fig. 1(b) leads to smaller leakage from the decoherence-free subspace, while for $H_{G,-}$ it is better to employ the central gate U_{CZ}.

We next consider a more general class of Hamiltonian distortions of the form

$$H_{G,\pm} = H_G + \frac{\kappa}{8}(H_B \otimes I \pm I \otimes H_D), \tag{13}$$

where H_B and H_D are random single-qubit Hamiltonians H generated such that each of the matrix elements $\langle 0|H|0\rangle$, $\langle 1|H|1\rangle$, $\mathrm{Re}\langle 0|H|1\rangle$, and $\mathrm{Im}\langle 0|H|1\rangle$ is drawn from a normal distribution with variance 1. In Fig. 3, we plot the relation between leakages L, operation differences D, and gate fidelities F for the central gates W and U_{CZ} for 1000 randomly generated Hamiltonian distortions. The graphs in Fig. 3 show that for about 50% errors from the considered class, gate W is superior as it leads to reduced leakage from the decoherence-free subspace, while the quality of the gate implemented on the states in the decoherence-free subspace, quantified by the gate fidelity F, is practically identical for W and U_{CZ}. This example confirms that

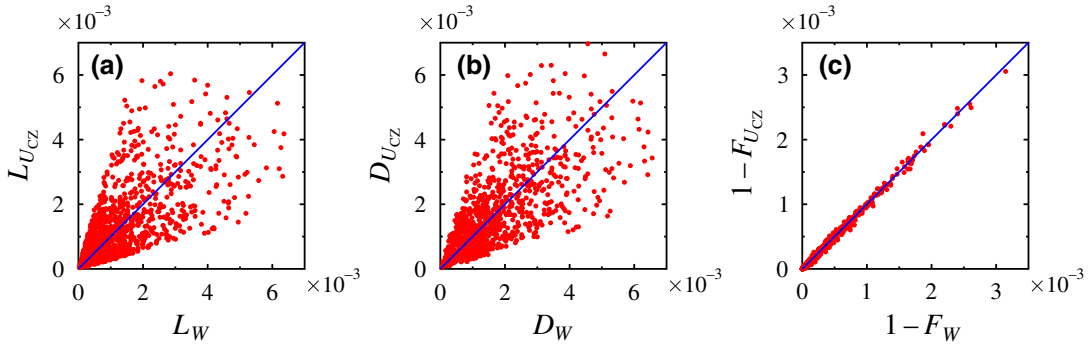

FIG. 3. The leakage L from the decoherence-free subspace (a), the difference D between the actually implemented operation and the ideal CNOT gate on the logical qubits (b), and the gate infidelities $1-F$ (c) are compared for the central gates W and U_{CZ} for 1000 randomly generated Hamiltonian distortions (see the main text) and $\kappa = 0.05$. The data are plotted as red dots. For reference, the blue line in each graph indicates the points at which the two plotted quantities coincide.

for certain kinds of errors and imperfections, it may be advantageous to utilize native four-qubit gates, provided that they are available, instead of two-qubit gates, when implementing operations on encoded logical qubits.

III. EXPERIMENTAL SETUP

We now proceed to the experimental test of the implementation of the CZ gate on logical qubits via a four-qubit gate W acting on physical qubits. The quantum logic circuit of our experiment is depicted in Fig. 4. At the input, two qubits, A and B, encode the quantum information and are prepared in pure states $|\psi\rangle_A$ and $|\varphi\rangle_B$, respectively. Two additional ancillary qubits, C and D, are prepared in state $|1\rangle$. Two quantum CNOT gates serve to encode the information into logical qubits and are supported by a pair of physical qubits; for instance, $(\alpha|0\rangle_A + \beta|1\rangle_A)|1\rangle_C \rightarrow \alpha|01\rangle_{AC} + \beta|10\rangle_{AC}$. Dephasing is imposed by single-qubit phase shift gates acting on each qubit. Collective dephasing occurs when the phase shifts applied to A and C (or B and D) are always identical, as indicated in the figure. The entangling CZ gate on the logical qubits is implemented via a four-qubit gate W on the physical qubits. Subsequently, we decode the logical qubits back to single physical qubits by performing measurements in the superposition basis $|\pm\rangle = \frac{1}{\sqrt{2}}(|0\rangle \pm |1\rangle)$ on qubits C and D. This quantum erasing directly maps the state of the logical qubit onto the physical qubit if the measurement result reads $|+\rangle$. In case of result $|-\rangle$, a compensating phase-flip operation σ_Z has to be applied to the physical qubit, which can be deterministically accomplished by a feed-forward operation [30–35].

Our experiment exploits the linear-optics platform [36, 37], which has proved extremely suitable for proof-of-principle tests of various quantum protocols, since it offers high purity of input states, very precise control, and high flexibility. In our experiment, frequency-degenerate time-correlated photon pairs with central wavelength 810 nm are generated in the process of spontaneous parametric down-conversion in a nonlinear β-barium borate (BBO) crystal pumped by a cw laser diode with central wavelength 405 nm. The orthogonally polarized signal and idler photons are spatially separated at a polarizing beam splitter and are guided via optical fibers to the input ports of our main setup, shown in Fig. 5, which is built from bulk-optics components and allows us to implement the four-qubit quantum CCCZ gate [38] or its variant W with suitable bit flips. The implementation of this gate is greatly simplified by our chosen hybrid qubit encoding, where each photon encodes two qubits: one in polarization and the other in path in an optical interferometer formed by a pair of calcite beam displacers. These two interferometers have differing spacing between the interferometer arms (4 mm and 6 mm, respectively). This ensures that only photons traveling in specific spatial modes overlap on the central partially

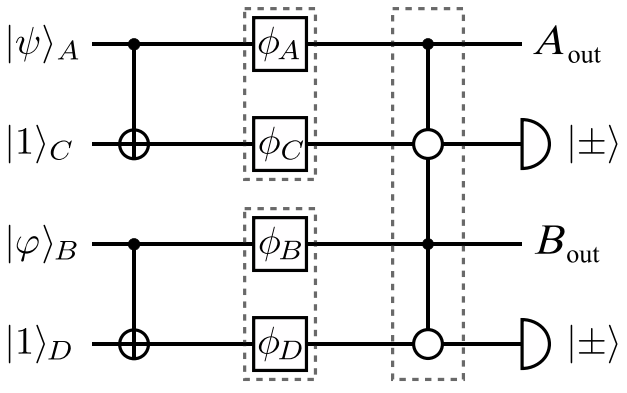

FIG. 4. A quantum logic circuit depicting the implementation of a two-qubit quantum CZ gate resilient to collective dephasing. Each logical qubit is encoded into a pair of physical qubits. The circuit involves two-qubit CNOT gates and a four-qubit W gate, defined in Eq. (5). The output auxiliary qubits, C and D, are measured in the superposition basis $|\pm\rangle$. Dephasing is modeled by random single-qubit phase shifts.

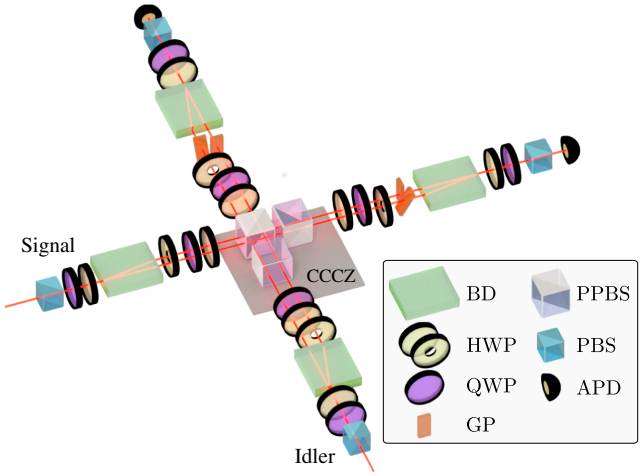

FIG. 5. The experimental setup. The interferometer is constructed from calcite beam displacers (BDs), partially polarized beam splitters (PBSs), half-wave plates (HWPs), quarter-wave plates (QWPs), and glass plates (GPs). The output polarization states of the single photons are analyzed with the use of wave plates and polarizing beam splitters (PBSs) and the photons are detected by avalanche photodiodes (APDs).

polarizing beam splitter (PPBS) that forms the core of the linear optical four-qubit CCCZ gate. The PPBS has reflectivity $R_H = 0$ for horizontal and $R_V = 2/3$ for vertical polarization. The other PPBSs serve to balance the amplitudes and have reflectivity $R_V = 0$ and $R_H = 2/3$. The polarization states are controlled by wave plates including ring-shaped wave plates that are utilized to address only a single arm of the Mach-Zehnder interferometer. The output photons are detected using avalanche photodiodes and various two-photon coincidences are recorded. The setup is inherently stable on a time scale of hours with an observed interferometric phase drift of 1°/h when the setup is appropriately shielded from airflow and kept at a stable temperature (fluctuation within $0.2\,^\circ$C), which enables the efficient collection of large amounts of experimental data. The states of photons A and B are initially encoded into polarization and the calcite beam displacers ensure the encoding of the logical qubit into a pair of physical qubits (the polarization and path qubit of a single photon). The single-qubit phase shifts can be implemented via suitable combinations of wave plates. To make our experimental implementation more efficient, we combine the (random) phase shifts with the state-preparation or measurement-basis selection, which reduces the number of required wave plates in the setup. More technical details on our setup can be found in our previous works [38–41].

TABLE I. The parameters of the four-qubit output states generated from input superposition states by the linear optical circuit that implements the four-qubit entangling gate W. The table shows the fidelity F of the experimental state with the ideal theoretical state, the purity of the output state $\mathcal{P}$, and the fidelity F_{opt} optimized by using the compensating single-qubit phase shifts that are determined from the tomographically reconstructed four-qubit density matrices. The numbers in parentheses represent one standard deviation.

$\lvert\Psi_{\text{in}}\rangle$	F	F_{opt}	$\mathcal{P}$
$\lvert+_L\rangle\lvert+_L\rangle = \lvert\Psi^+\rangle_{\text{AC}}\lvert\Psi^+\rangle_{\text{BD}}$	0.890(5)	0.936(5)	0.918(9)
$\lvert+_L\rangle\lvert-_L\rangle = \lvert\Psi^+\rangle_{\text{AC}}\lvert\Psi^-\rangle_{\text{BD}}$	0.937(4)	0.942(4)	0.930(7)
$\lvert-_L\rangle\lvert+_L\rangle = \lvert\Psi^-\rangle_{\text{AC}}\lvert\Psi^+\rangle_{\text{BD}}$	0.924(4)	0.934(4)	0.923(8)
$\lvert-_L\rangle\lvert-_L\rangle = \lvert\Psi^-\rangle_{\text{AC}}\lvert\Psi^-\rangle_{\text{BD}}$	0.932(4)	0.938(4)	0.928(8)

We characterize the generated two-qubit and four-qubit quantum states via full quantum state tomography [42]. Each qubit is measured in three mutually unbiased bases comprising the computational basis $\{|0\rangle, |1\rangle\}$ and two superposition bases, $\frac{1}{\sqrt{2}}(|0\rangle \pm |1\rangle)$ and $\frac{1}{\sqrt{2}}(|0\rangle \pm i|1\rangle)$. The total number of measurements, N, thus reads 36 for two-qubit states and 1296 for four-qubit states. Let

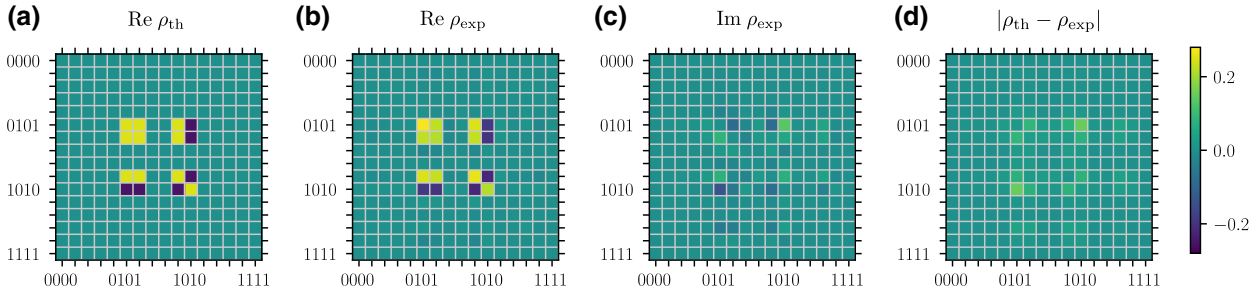

FIG. 6. The theoretical and experimental density matrices of a four-qubit state produced from input state $|\Psi^+\rangle|\Psi^+\rangle$ by the linear optical quantum gate W. The real part of the theoretical density matrix is shown in (a) and its imaginary part exactly vanishes. (b),(c) The real and imaginary parts of the experimentally reconstructed density matrix, respectively. (d) The difference between the theoretical and experimental density matrices, $|\Delta\rho| = |\rho_{\text{th}} - \rho_{\text{exp}}|$. All the nonzero density-matrix elements of ρ_{th} have absolute value 0.25. The maximum difference between the matrix elements of ρ_{th} and ρ_{exp} occurs for the off-diagonal element $\rho_{0101,1010}$, $|\Delta\rho_{0101,1010}| = 0.149$ and is caused mainly by phase discrepancies, as indicated by the nonzero imaginary part of ρ_{exp}.

TABLE II. The experimental fidelities and entanglement of formation of output states of qubits A and B for input state $|+\rangle|+\rangle$ and the full collective dephasing acting on pairs of qubits A and C ($F^A_{\rm AB}$, $E^A_{\rm AB}$) and B and D ($F^B_{\rm AB}$, $E^B_{\rm AB}$) or both A and C and B and D ($F^{\rm AB}_{\rm AB}$, $E^{\rm AB}_{\rm AB}$). The entanglement of formation and the fidelities are shown for four different outcomes of measurements on output qubits C and D.

$\|{\rm CD}\rangle$	$F^A_{\rm AB}$	$F^B_{\rm AB}$	$F^{\rm AB}_{\rm AB}$	$E^A_{\rm AB}$	$E^B_{\rm AB}$	$E^{\rm AB}_{\rm AB}$
$\|++\rangle$	0.920(9)	0.930(9)	0.947(5)	0.87(2)	0.92(2)	0.90(1)
$\|+-\rangle$	0.961(6)	0.962(5)	0.960(4)	0.91(1)	0.92(2)	0.91(1)
$\|-+\rangle$	0.888(8)	0.912(7)	0.918(6)	0.84(2)	0.86(2)	0.87(2)
$\|--\rangle$	0.911(7)	0.918(7)	0.921(5)	0.88(2)	0.88(2)	0.89(1)

$\{\Pi_n\}_{n=1}^N$ represent the projectors describing the tomographic measurement and let f_n denote the number of measured two-photon coincidence counts for projection Π_n. We reconstruct the quantum state ρ by an iterative maximum-likelihood-estimation algorithm [43], which seeks the maximum of the likelihood function $\mathcal{L} = \prod_{n=1}^N p_n^{f_n}$ under the constraints $\rho \geq 0$ and ${\rm Tr}\,\rho = 1$. Here, $p_n = {\rm Tr}[\rho\Pi_n]$ is the theoretical probability of measurement outcome Π_n. The iteration formula for ρ that maximizes $\mathcal{L}$ reads

$$\rho_{j+1} = \frac{R_j\,\rho_j\,R_j}{{\rm Tr}[R_j\,\rho_j\,R_j]}, \quad R_j = \sum_{n=1}^{N} \frac{f_n}{{\rm Tr}[\rho_j\,\Pi_n]}\Pi_n. \tag{14}$$

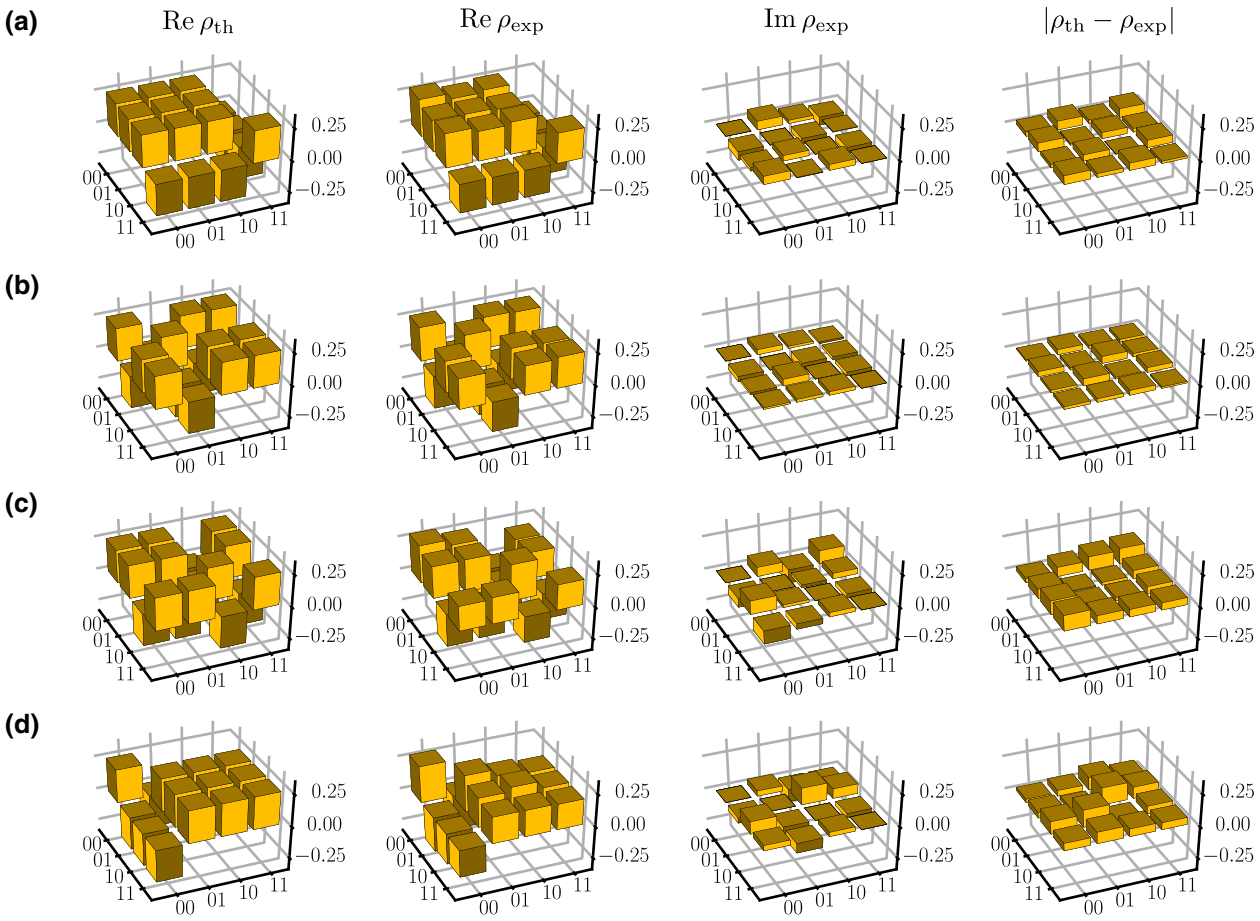

FIG. 7. The theoretical (leftmost column) and experimental (middle columns) density matrices of output two-qubit states of A and B for decoherence-resilient implementation of the $U_{\rm CZ}$ gate under full collective dephasing. The imaginary parts of all plotted theoretical density matrices vanish. To facilitate comparison between theory and experiment, the absolute value of $\rho_{\rm th} - \rho_{\rm exp}$ is plotted in the rightmost column. The results are shown for superposition input state $|+_L\rangle|+_L\rangle = |\Psi^+\rangle|\Psi^+\rangle$ and for four different measurement results on qubits C and D: (a) $++$, (b) $+-$, (c) $-+$, and (d) $--$.

TABLE III. The same as Table II but the dephasing acts only on single qubits A and B, while qubits C and D remain intact.

$\|CD\rangle$	F^A_{AB}	F^B_{AB}	F^{AB}_{AB}	E^A_{AB}	E^B_{AB}	E^{AB}_{AB}
$\|++\rangle$	0.44(1)	0.47(1)	0.25(1)	0.005(5)	0.07(2)	0
$\|+-\rangle$	0.48(1)	0.50(1)	0.27(1)	0.010(7)	0.07(1)	0
$\|-+\rangle$	0.46(1)	0.46(1)	0.25(1)	0.001(4)	0.05(1)	0
$\|--\rangle$	0.46(1)	0.48(1)	0.26(1)	0.001(4)	0.06(1)	0

This iterative procedure exhibits good convergence and several hundreds of iterations are typically sufficient to reach the stationary point that maximizes $\mathcal{L}$.

IV. EXPERIMENTAL RESULTS

We first check the action of the four-qubit W gate on the input superposition states obtained by preparing both qubits A and B in states $|\pm\rangle$. In this case, the four-qubit unitary operation W should produce a maximally entangled state of the two logical qubits. At the level of physical qubits, the inputs correspond to products of Bell states $|\Psi^{\pm}\rangle = \frac{1}{\sqrt{2}}(|01\rangle \pm |10\rangle)$ (see Table I). As an example, consider the input state $|\Psi_{in}\rangle = |\Psi^+\rangle|\Psi^+\rangle$. The corresponding output state of the four physical qubits reads

$$|\Psi_{out}\rangle = \frac{1}{2}(|0101\rangle + |1001\rangle + |0110\rangle - |1010\rangle). \quad (15)$$

We plot the density matrix of the output state reconstructed from the experimental data in Fig. 6 together with the theoretical density matrix of the ideal output pure state $|\Psi_{out}\rangle\langle\Psi_{out}|$. Clear agreement between the theory and experiment can be seen. We characterize the quality of the output four-qubit states ρ by their purity $\mathcal{P} = \mathrm{Tr}[\rho^2]$ and fidelity $F = \langle\Psi_{out}|\rho|\Psi_{out}\rangle$, where $|\Psi_{out}\rangle$ is the ideal pure output state. The data are listed in Table I and we can see that a fidelity typically exceeding 90% is achieved. The fidelity can be further improved if we compensate for residual single-qubit phase shifts; see the F_{opt} column in Table I. The statistical errors indicated in the table are estimated from the measured two-photon coincidence counts assuming their Poissonian statistics and using the bootstrapping method [39,44] with 1000 samples.

After checking the performance of our quantum logic circuit, we proceed with the main experimental test of the quantum gate that is resilient to dephasing. We again choose to test the gate for input superposition state $|+_L\rangle|+_L\rangle$, since this state is the most sensitive to dephasing. We consider full dephasing, $q = 1/2$, which is modeled as a balanced mixture of the identity operation and the phase flip σ_Z. Collective dephasing means that the phase shifts on two qubits (A and C or B and D) are identical, $\phi_A = \phi_C$ and $\phi_B = \phi_D$, respectively. We consider dephasing of one pair of physical qubits and also independent dephasing of both pairs of physical qubits. For instance, in the case of collective dephasing on both pairs of qubits, the experimentally recorded two-photon coincidences combine data corresponding to four different phase shifts: $\phi_A = 0$ and $\phi_B = 0$, $\phi_A = \pi$ and $\phi_B = 0$, $\phi_A = 0$ and $\phi_B = \pi$, $\phi_A = \pi$ and $\phi_B = \pi$. In all cases, $\phi_A = \phi_C$ and $\phi_B = \phi_D$ hold. We measure the output qubits C and D in the superposition basis $|\pm\rangle$ and for each of the four combinations of measurement outputs we reconstruct, from the experimental data, the two-qubit density matrix of the output state of qubits A and B. Up to single-qubit phase flips, we should obtain a pure maximally entangled two-qubit state $U_{CZ}|+\rangle|+\rangle$, provided that the protection against dephasing is functional.

The results are summarized in Table II, where we display the fidelities and the entanglement of formation [45] of the output two-qubit state of A and B for the three different combinations of dephasing and four different measurement outcomes on qubits C and D. In all cases, we achieve very high fidelities and preserved entanglement, which clearly confirms the protection from dephasing and also illustrates that a feed-forward operation could be used to recover the correct output state of qubits A and B for any combination of measurement outcomes on qubits C and D. In Fig. 7, we plot the output density matrices of two-qubit states of A and B obtained for independent collective dephasing on both pairs of qubits. This figure further confirms the closeness between the theoretical expectations and the experimental results and it also depicts the

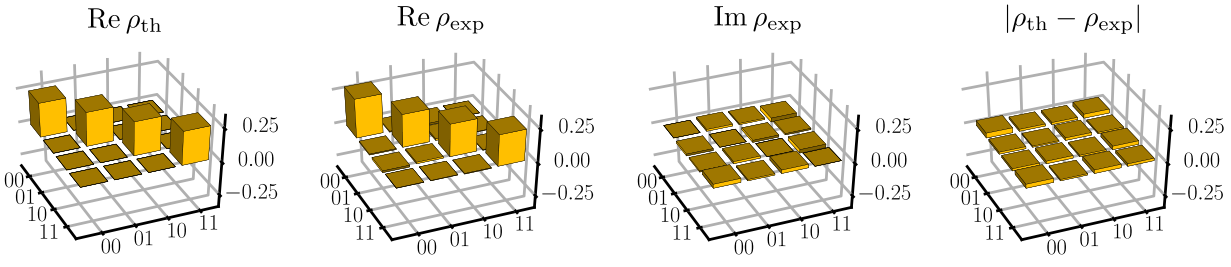

FIG. 8. The same as Fig. 7(a) but the dephasing acts only on qubits A and B and so the output state is affected by decoherence and becomes very close to the maximally mixed state.

single-qubit phase flips imposed by measurements on qubits C and D.

Let us now discuss the main experimental imperfections leading to reduced quantum state fidelities and purities. The purity is primarily reduced due to the partial distinguishability of the signal and idler photons, which is caused by imperfect spatial, temporal, and spectral mode matching. This partial distinguishability results in imperfect two-photon interference on the central partially polarizing beam splitter in the experimental setup, which also causes an imbalance of the diagonal elements of the density matrix. Specifically, the success probability of the gate for two vertically polarized photons becomes higher than for the other polarizations due to the weaker destructive interference on the central PPBS. The secondary cause of purity reduction is the finite visibility of the calcite interferometers. The imperfect classical visibility is caused by the different wavefront errors accumulated in each interferometer path and the unequal length of the calcite crystals. A slight difference in the length of the calcite crystals causes the recombined beams not to overlap exactly, due to the slight respective lateral shift. Fast interferometric phase fluctuations also add to decoherence and purity reduction.

Another effect causing reduction of state fidelity is represented by unwanted phase shifts, indicated by imaginary parts of the reconstructed density matrices. These phase shifts are partly induced by a slow drift of the interferometric phase during the measurement, which also leads to dephasing. The imperfect and uncompensated retardances of the wave plates used for state preparation and manipulation also cause unwanted phase shifts. Together with the imperfect angular alignment of the wave plates, these retardance imperfections also influence the balance of amplitudes and introduce extra nonzero density-matrix elements in the prepared four-qubit states (see Fig. 6). Moreover, imperfect beam-splitting ratios cause an additional slight disbalance of the amplitudes.

For the four-qubit output quantum states the fidelities of which are listed in Table I, an analysis of the reconstructed density matrices reveals that the decoherence and loss of purity contributes to fidelity reduction by 3.9%, on average. The unbalancing of the state amplitudes and the emergence of extra nonzero density-matrix elements reduces the fidelity by an additional 2.5% on average. The influence of unwanted deterministic phase shifts varies rather significantly from state to state and results in fidelity reduction in the interval from 0.5% to 4.6%. Among the 4 states listed in Table I, the effect of unwanted phase shifts is most pronounced for the state plotted in Fig. 6, as can be seen from the table by comparing the fidelities F and F_{opt}.

As a benchmark and to illustrate the importance of collective dephasing, we perform reference measurements in which the dephasing is always applied only to one of the two physical qubits encoding a logical qubit. Specifically, $\phi_C = \phi_D = 0$ is set throughout the whole measurement, while ϕ_A and ϕ_B is set to 0 or π as required to apply dephasing to a given qubit. In this case, the encoding is of no use and the output state suffers from loss of coherence. In Table III, we provide the same data as in Table II but for dephasing acting on qubits A and B only. We can see that the entanglement practically vanishes and the fidelities drop significantly due to decoherence. Theoretically, entanglement is completely erased by such dephasing, $E = 0$, and we expect fidelity $\frac{1}{2}$ for decoherence on a single qubit and $\frac{1}{4}$ for decoherence on both qubits. Our experimental results are in good agreement with these theoretical predictions. In Fig. 8, we give an example of the output density matrix of qubits A and B when they both suffer from complete dephasing. The decoherence washes out all off-diagonal elements of the density matrix and the state becomes very close to the maximally mixed state.

V. CONCLUSIONS

In summary, we successfully experimentally test the optical implementation of a maximally entangling quantum CZ gate that is resilient to collective dephasing. The quantum information is protected from the collective decoherence by encoding each logical qubit into a pair of physical qubits. Our work illustrates the potential importance and usefulness of inherently multiqubit quantum gates for quantum-information processing within decoherence-free subspaces. In our experiment, the quantum CZ gate on logical qubits is realized by applying a suitable gate to all four physical qubits. We show theoretically that in the presence of additional noise or imperfections beyond collective dephasing, the approach exploiting native multiqubit gates can be advantageous in comparison to applying a gate to two physical qubits only. Our study thus indicates the potential advantages of circuit-specific optimization of decoherence-free gate architecture that takes into account errors in the other gates in the circuit. The studied approach is suitable for any physical architecture in which native multiqubit gates can be implemented. The method is not limited to the quantum CZ gate and can be extended to other entangling gates and also to other noise models if some nontrivial decoherence-free subspace can be identified in the Hilbert space of the physical qubits. Since implementations of linear optical quantum gates are probabilistic and the overheads typically grow rapidly with the increasing number of qubits, we anticipate that the proposed utilization of multiqubit gates could find application mainly in atomic and solid-state quantum-information processing architectures. Nevertheless, we would like to point out the recent significant progress in the design of integrated quantum photonic circuits [46] and feed-forward-enhanced multiplexed heralded sources of single

photons [47]. These advances indicate that even very complex photonic quantum processors addressing several tens of photons simultaneously can be achievable in the future, finding applications in, e.g., advanced optical quantum communication networks.

ACKNOWLEDGMENTS

This work was supported by the Czech Science Foundation (Grant No. GA16-17314S). R.F. also acknowledges funding from the MEYS and funding from the European Union Horizon 2020 (2014–2020) Research and Innovation framework program, under Grant Agreement No. 731473 (project No. 8C20002 ShoQC). Project ShoQC has received funding from the QuantERA ERA-NET Cofund in Quantum Technologies implemented within the European Union Horizon 2020 program.

[1] P. W. Shor, Scheme for reducing decoherence in quantum computer memory, Phys. Rev. A **52**, R2493 (1995).
[2] A. M. Steane, Multiple particle interference and quantum error correction, Proc. R. Soc. Lond. A **452**, 2551 (1996).
[3] A. R. Calderbank and P. W. Shor, Good quantum error-correcting codes exist, Phys. Rev. A **54**, 1098 (1996).
[4] M. A. Nielsen and I. L. Chuang, *Quantum Computation and Quantum Information* (Cambridge University Press, Cambridge, UK, 2000).
[5] X.-C. Yao, T.-X. Wang, H.-Z. Chen, W.-B. Gao, A. G. Fowler, R. Raussendorf, Z.-B. Chen, N.-L. Liu, C.-Y. Lu, Y.-J. Deng, Y.-A. Chen, and J.-W. Pan, Experimental demonstration of topological error correction, Nature **482**, 489 (2012).
[6] B. A. Bell, D. A. Herrera-Martí, M. S. Tame, D. Markham, W. J. Wadsworth, and J. G. Rarity, Experimental demonstration of graph-state quantum secret sharing, Nat. Commun. **5**, 3658 (2014).
[7] D. P. DiVincenzo, The physical implementation of quantum computation, Fortschritte der Physik **48**, 771 (2000).
[8] E. Knill, Quantum computing with realistically noisy devices, Nature **434**, 39 (2005).
[9] T. Monz, D. Nigg, E. A. Martinez, M. F. Brandl, P. Schindler, R. Rines, S. X. Wang, I. L. Chuang, and R. Blatt, Realization of a scalable Shor algorithm, Science **351**, 1068 (2016).
[10] F. Arute *et al.*, Quantum supremacy using a programmable superconducting processor, Nature **574**, 505 (2019).
[11] L.-M. Duan and G.-C. Guo, Preserving Coherence in Quantum Computation by Pairing Quantum Bits, Phys. Rev. Lett. **79**, 1953 (1997).
[12] P. Zanardi and M. Rasetti, Noiseless Quantum Codes, Phys. Rev. Lett. **79**, 3306 (1997).
[13] D. A. Lidar, I. L. Chuang, and K. B. Whaley, Decoherence-Free Subspaces for Quantum Computation, Phys. Rev. Lett. **81**, 2594 (1998).
[14] P. G. Kwiat, A. J. Berglund, J. B. Altepeter, and A. G. White, Experimental verification of decoherence-free subspaces, Science **290**, 498 (2000).
[15] J. Kempe, D. Bacon, D. A. Lidar, and K. B. Whaley, Theory of decoherence-free fault-tolerant universal quantum computation, Phys. Rev. A **63**, 042307 (2001).
[16] M. Bourennane, M. Eibl, S. Gaertner, C. Kurtsiefer, A. Cabello, and H. Weinfurter, Decoherence-Free Quantum Information Processing with Four-Photon Entangled States, Phys. Rev. Lett. **92**, 107901 (2004).
[17] R. Blume-Kohout, H. K. Ng, D. Poulin, and L. Viola, Characterizing the Structure of Preserved Information in Quantum Processes, Phys. Rev. Lett. **100**, 030501 (2008).
[18] D. A. Lidar, Review of decoherence free subspaces, noiseless subsystems, and dynamical decoupling, Adv. Chem. Phys. **154**, 295 (2014).
[19] H. Lu, L.-K. Chen, C. Liu, P. Xu, X.-C. Yao, L. Li, N.-L. Liu, B. Zhao, Y.-A. Chen, and J.-W. Pan, Experimental realization of a concatenated Greenberger-Horne-Zeilinger state for macroscopic quantum superpositions, Nat. Photonics **8**, 364 (2014).
[20] T. Monz, K. Kim, A. S. Villar, P. Schindler, M. Chwalla, M. Riebe, C. F. Roos, H. Häffner, W. Hänsel, M. Hennrich, and R. Blatt, Realization of Universal Ion-Trap Quantum Computation with Decoherence-Free Qubits, Phys. Rev. Lett. **103**, 200503 (2009).
[21] R. Ikuta, Y. Ono, T. Tashima, T. Yamamoto, M. Koashi, and N. Imoto, Efficient Decoherence-Free Entanglement Distribution over Lossy Quantum Channels, Phys. Rev. Lett. **106**, 110503 (2011).
[22] T. Yamamoto, J. Shimamura, S. K. Özdemir, M. Koashi, and N. Imoto, Faithful Qubit Distribution Assisted by One Additional Qubit against Collective Noise, Phys. Rev. Lett. **95**, 040503 (2005).
[23] R. Prevedel, M. S. Tame, A. Stefanov, M. Paternostro, M. S. Kim, and A. Zeilinger, Experimental Demonstration of Decoherence-Free One-Way Information Transfer, Phys. Rev. Lett. **99**, 250503 (2007).
[24] T. Yamamoto, K. Hayashi, S. K. Özdemir, M. Koashi, and N. Imoto, Robust photonic entanglement distribution by state-independent encoding onto decoherence-free subspace, Nat. Photonics **2**, 488 (2008).
[25] L. Aolita, L. Davidovich, K. Kim, and H. Häffner, Universal quantum computation in decoherence-free subspaces with hot trapped ions, Phys. Rev. A **75**, 052337 (2007).
[26] W.-H. Zurek, Decoherence, einselection, and the quantum origins of the classical, Rev. Mod. Phys. **75**, 715 (2003).
[27] J. L. O'Brien, G. J. Pryde, A. Gilchrist, D. F. V. James, N. K. Langford, T. C. Ralph, and A. G. White, Quantum Process Tomography of a Controlled-NOT Gate, Phys. Rev. Lett. **93**, 080502 (2004).
[28] A. Gilchrist, N. K. Langford, and M. A. Nielsen, Distance measures to compare real and ideal quantum processes, Phys. Rev. A **71**, 062310 (2005).
[29] M. Sedlák and J. Fiurášek, Generalized Hofmann quantum process fidelity bounds for quantum filters, Phys. Rev. A **93**, 042316 (2016).
[30] S. Giacomini, F. Sciarrino, E. Lombardi, and F. De Martini, Active teleportation of a quantum bit, Phys. Rev. A **66**, 030302(R) (2002).
[31] M. Riebe, H. Häffner, C. F. Roos, W. Hänsel, J. Benhelm, G. P. T. Lancaster, T. W. Körber, C. Becher, F. Schmidt-Kaler, D. F. V. James, and R. Blatt, Deterministic

quantum teleportation with atoms, Nature **429**, 734 (2004).
[32] R. Prevedel, P. Walther, F. Tiefenbacher, P. Böhi, R. Kaltenbaek, T. Jennewein, and A. Zeilinger, High-speed linear optics quantum computing using active feed-forward, Nature **445**, 65 (2007).
[33] M. Miková, H. Fikerová, I. Straka, M. Mičuda, J. Fiurášek, M. Ježek, and M. Dušek, Increasing efficiency of a linear-optical quantum gate using electronic feed-forward, Phys. Rev. A **85**, 012305 (2012).
[34] L. Steffen, Y. Salathe, M. Oppliger, P. Kurpiers, M. Baur, C. Lang, C. Eichler, G. Puebla-Hellmann, A. Fedorov, and A. Wallraff, Deterministic quantum teleportation with feed-forward in a solid state system, Nature **500**, 319 (2013).
[35] W. Pfaff, B. J. Hensen, H. Bernien, S. B. van Dam, M. S. Blok, T. H. Taminiau, M. J. Tiggelman, R. N. Schouten, M. Markham, D. J. Twitchen, and R. Hanson, Unconditional quantum teleportation between distant solid-state quantum bits, Science **345**, 532 (2014).
[36] P. Kok, W. J. Munro, K. Nemoto, T. C. Ralph, J. P. Dowling, and G. J. Milburn, Linear optical quantum computing with photonic qubits, Rev. Mod. Phys. **79**, 135 (2007).
[37] J.-W. Pan, Z.-B. Chen, C.-Y. Lu, H. Weinfurter, A. Zeilinger, and M. Zukowski, Multiphoton entanglement and interferometry, Rev. Mod. Phys. **84**, 777 (2012).
[38] R. Stárek, M. Mičuda, M. Miková, I. Straka, M. Dušek, M. Ježek, and J. Fiurášek, Experimental investigation of a four-qubit linear-optical quantum logic circuit, Sci. Rep. **6**, 33475 (2016).
[39] R. Stárek, M. Miková, I. Straka, M. Dušek, M. Ježek, J. Fiurášek, and M. Mičuda, Experimental realization of SWAP operation on hyper-encoded qubits, Opt. Express **26**, 8443 (2018).
[40] R. Stárek, M. Mičuda, I. Straka, M. Miková, M. Ježek, R. Filip, and J. Fiurášek, Control and enhancement of interferometric coupling between two photonic qubits, Phys. Rev. A **93**, 042321 (2016).
[41] M. Mičuda, M. Sedlák, I. Straka, M. Miková, M. Dušek, M. Ježek, and J. Fiurášek, Efficient Experimental Estimation of Fidelity of Linear Optical Quantum Toffoli Gate, Phys. Rev. Lett. **111**, 160407 (2013).
[42] *Quantum State Estimation*, edited by M. Paris and J. Řeháček, Lecture Notes in Physics Vol. 649 (Springer, Heidelberg, 2004).
[43] M. Ježek, J. Fiurášek, and Z. Hradil, Quantum inference of states and processes, Phys. Rev. A **68**, 012305 (2003).
[44] B. Efron and R. J. Tibshirani, *An Introduction to the Bootstrap* (Chapman and Hall, London, 1994).
[45] W. K. Wootters, Entanglement of Formation of an Arbitrary State of Two Qubits, Phys. Rev. Lett. **80**, 2245 (1998).
[46] J. Wang, F. Sciarrino, A. Laing, and M. G. Thompson, Integrated photonic quantum technologies, Nat. Photonics **14**, 273 (2020).
[47] E. Meyer-Scott, C. Silberhorn, and A. Migdall, Single-photon sources: Approaching the ideal through multiplexing, Rev. Sci. Instrum. **91**, 041101 (2020).